Dynamic Changes between Two LHCX-Related Energy Quenching Sites Control Diatom Photoacclimation[1]

Lucilla Taddei,[a] Volha U. Chukhutsina,[b,c] Bernard Lepetit,[d] Giulio Rocco Stella,[a,e] Roberto Bassi,[e] Herbert van Amerongen,[b] Jean-Pierre Bouly,[a] Marianne Jaubert,[a] Giovanni Finazzi,[f,2] and Angela Falciatore[a,2]

[a]Sorbonne Université, Centre National de la Recherche Scientifique, Institut de Biologie Paris-Seine, Laboratory of Computational and Quantitative Biology, F-75005 Paris, France
[b]Laboratory of Biophysics and MicroSpectroscopy Research Facility, Wageningen University, 6700ET Wageningen, The Netherlands
[c]Biophysics of Photosynthesis, Department of Physics and Astronomy, Faculty of Sciences, Vrije Universiteit Amsterdam and LaserLaB Amsterdam, 1081 HV Amsterdam, The Netherlands
[d]Zukunftskolleg, Department of Plant Ecophysiology, University of Konstanz, 78457 Konstanz, Germany
[e]Department of Biotechnology, University of Verona, I-37134 Verona, Italy
[f]Université Grenoble Alpes, Laboratoire de Physiologie Cellulaire et Végétale, Unité Mixte de Recherche 5168, Centre National de la Recherche Scientifique, Institut National Recherche Agronomique, Commissariat à l'Energie Atomique et aux Energies Alternatives, Institut de Biosciences et Biotechnologies de Grenoble, CEA Grenoble, F-38054 Grenoble cedex 9, France

ORCID IDs: 0000-0003-3841-6186 (L.T.); 0000-0003-0304-5573 (V.U.C.); 0000-0001-9980-9210 (B.L.); 0000-0001-6852-0967 (G.R.S.); 0000-0002-4140-8446 (R.B.); 0000-0002-9783-2895 (H.v.A.); 0000-0002-2423-3867 (J.B.); 0000-0001-5419-5796 (M.J.); 0000-0003-0597-7075 (G.F.); 0000-0003-3318-9578 (A.F.)

Marine diatoms are prominent phytoplankton organisms that perform photosynthesis in extremely variable environments. Diatoms possess a strong ability to dissipate excess absorbed energy as heat via nonphotochemical quenching (NPQ). This process relies on changes in carotenoid pigment composition (xanthophyll cycle) and on specific members of the light-harvesting complex family specialized in photoprotection (LHCXs), which potentially act as NPQ effectors. However, the link between light stress, NPQ, and the existence of different LHCX isoforms is not understood in these organisms. Using picosecond fluorescence analysis, we observed two types of NPQ in the pennate diatom *Phaeodactylum tricornutum* that were dependent on light conditions. Short exposure of low-light-acclimated cells to high light triggers the onset of energy quenching close to the core of photosystem II, while prolonged light stress activates NPQ in the antenna. Biochemical analysis indicated a link between the changes in the NPQ site/mechanism and the induction of different LHCX isoforms, which accumulate either in the antenna complexes or in the core complex. By comparing the responses of wild-type cells and transgenic lines with a reduced expression of the major LHCX isoform, LHCX1, we conclude that core complex-associated NPQ is more effective in photoprotection than is the antenna complex. Overall, our data clarify the complex molecular scenario of light responses in diatoms and provide a rationale for the existence of a degenerate family of LHCX proteins in these algae.

[1]This work was supported by the Marie Curie Initial Training Network Accliphot (FP7-PEPOPLE-2012- ITN; 316427) to A.F., G.F., and R.B., the Agence Nationale de la Recherche (ANR-12-BIME DiaDomOil) to A.F. and G.F., the Marie Curie Initial Training Network CALIPSO (ITN 2013 GA 607607) to A.F., the Human Frontier Science Program (HFSP0052) and the LabEx GRAL (ANR-10-LABX-49-01) to G.F., and the Zukunftskolleg Konstanz and the Deutsche Forschungsgemeinschaft (DFG-LE 3358/3-1) to B.L.

[2]Address correspondence to giovanni.finazzi@cea.fr or angela.falciatore@upmc.fr.

The author responsible for distribution of materials integral to the findings presented in this article in accordance with the policy described in the Instructions for Authors (www.plantphysiol.org) is: Angela Falciatore (angela.falciatore@upmc.fr).

A.F., G.F., H.v.A., J.-P.B., M.J., B.L., and V.U.C. designed the experiments and wrote the article; L.T., M.J., B.L., A.F., J.-P.B., and G.F., contributed to the molecular and physiological analyses; G.R.S. and R.B. performed the pigment analysis; V.U.C. and H.v.A. analyzed quenching features and generated decay-associated spectra; all authors discussed results and revised and approved the article.

www.plantphysiol.org/cgi/doi/10.1104/pp.18.00448

Marine diatoms form a group of unicellular algae that dominate the phytoplankton community across a wide range of ocean environments (Smetacek, 1999; de Vargas et al., 2015; Malviya et al., 2016). Their environmental success likely reflects their capacity to respond to numerous environmental challenges, including changes in nutrient levels and light. While the mechanisms of the responses of diatoms to nutrients have been studied in detail (Allen et al., 2008, 2011; Marchetti et al., 2012; Alipanah et al., 2015; Morrissey et al., 2015; Matthijs et al., 2016; McQuaid et al., 2018), little is known about light acclimation responses. Like most photosynthetic organisms, diatoms optimize light capture by enhancing their absorption capacity at low intensities and by down-regulating the utilization of absorbed light at oversaturating energy fluxes (Müller et al., 2001; Eberhard et al., 2008). The latter process is triggered by the induction of the high-energy quenching (qE) component of nonphotochemical quenching (NPQ;

Horton et al., 1996). qE reflects the increased thermal dissipation of excess light following the activation of qE effector proteins in PSII and changes in the pigment composition (via carotenoid deepoxidation through the xanthophyll cycle). qE effectors include the small PSII subunit (PsbS) in plants and members of the light-harvesting complex stress-related (LHCSR) family in microalgae and mosses (Peers et al., 2009; Alboresi et al., 2010; Ballottari et al., 2016). The qE machinery of diatoms differs from that of plants and green algae in two main respects. Diatoms possess two xanthophyll cycles catalyzing the deepoxidation of diadinoxanthin (DD) to diatoxanthin (DT) and of violaxanthin (V) to zeaxanthin (Z; Lohr and Wilhelm, 1999). Moreover, their qE effectors belong to the light-harvesting complex (LHC) family specialized in photoprotection, the LHCX (Bailleul et al., 2010; Zhu and Green, 2010; Ghazaryan et al., 2016), which is related, but not identical, to the LHCSR family. Multiple LHCX genes exist in diatoms, and gene expression studies indicate that the four *Phaeodactylum tricornutum* LHCX isoforms differentially accumulate in the thylakoids upon exposure to different environmental stresses due to the existence of multiple regulatory control pathways (Allen et al., 2008; Nymark et al., 2009; Bailleul et al., 2010; Lepetit et al., 2013, 2017). These findings suggest that the functional diversity of the LHCX proteins may expand the diatom's capacity to respond to the highly variable ocean environments (Zhu and Green, 2010; Taddei et al., 2016; Lepetit et al., 2017).

In this work, we combined biochemical and spectroscopic approaches to address the roles of the different LHCXs in photoprotection. We found that low light (LL)-acclimated cells display a qE driven mainly by energy quenching in close proximity to the reaction center of PSII (the PSII core) and, to some extent, in the antennas (also called Fucoxanthin Complex Binding Proteins [FCPs]). This qE is largely controlled by LHCX1, which is present in both the PSII core and the FCP complexes. On the other hand, prolonged exposure to high light (HL) enhances FCP-localized quenching. Biochemical analysis suggests that this shift is related to the induction of other LHCX isoforms, which accumulate in the antenna but not in the PSII core. By comparing the physiological responses of wild-type and knockdown lines with reduced content of the LHCX1 isoform, we conclude that qE antenna quenching is less effective than core qE in protecting cells from light damage. Overall, by relating different qE mechanisms to different molecular actors, we propose a detailed model for diatom NPQ, which is one of the key elements of the environmental flexibility of these algae in modern oceans.

RESULTS

The LHCX1 Knockdown Line Recovers Wild-Type NPQ Levels upon Prolonged HL Exposure

In *P. tricornutum*, LHCX1 is the only member of the *LHCX* gene family that is expressed substantially in cells grown in LL (30 µmol photons m^{-2} s^{-1}, 12/12-h light/dark cycle; Bailleul et al., 2010; Taddei et al., 2016; Lepetit et al., 2017). In these conditions, LHCX1 is the main NPQ effector. This role is evidenced by the phenotype of a transgenic line with down-regulated expression of *LHCX1* (hereafter named *lhcx1*), which contained less LHCX1 and showed a lower qE capacity than the wild type when grown in LL (Bailleul et al., 2010; Fig. 1A; Supplemental Fig. S1). Exposure to HL (500 µmol photons m^{-2} s^{-1}, 12/12-h light/dark cycle; Fig. 1B) for 2 d enhanced NPQ in both wild-type and transgenic cells. However, the NPQ increase was larger in the mutant; therefore, the quenching capacity of the two strains became indistinguishable in HL. Immunoblot analysis of HL-treated cells showed that LHCX1 levels were increased in both strains, even if the *lhcx1* knockdown cells maintained a lower LHCX1 content than the wild-type cells (Fig. 1C). This observation suggests that the increase in LHCX1 alone cannot account for the observed difference in NPQ amplitude in LL- and HL-treated cells. To further elucidate the effect of quenching on antenna protein domains, we compared the xanthophyll cycle pigments in wild-type and *lhcx1* cells in LL and HL and found a similar DD/DT content in LL-treated cells (Supplemental Table S1), which was in agreement with previous results (Bailleul et al., 2010). HL triggered a significant increase of DD+DT but also led to the appearance of V, antheraxanthin (A), and Z (i.e. xanthophyll precursors of DD+DT synthesis under HL stress; Lohr and Wilhelm, 1999). The *lhcx1* knockdown line displayed a slightly increased amount of total DD+DT compared with the wild type, while its deepoxidation state was the same as that of the wild type. This increase of DT, in principle, could account for the recovery of wild-type-like NPQ levels in the *lhcx1* cells. Nevertheless, previous work has shown that the induction of DT by prolonged light stress cannot enhance NPQ without a concomitant increase of LHCX proteins (Bailleul et al., 2010; Lepetit et al., 2013, 2017). On the other hand, we detected a substantial accumulation of LHCX3 in both strains in HL (Fig. 1C). Induction of the LHCX2 isoform also was visible at the mRNA level (Fig. 1E) and at the protein level after overexposure of the western-blot membrane (Fig. 1D). Because of their possible role in NPQ, this finding prompted us to further investigate the link between the induction of these proteins and the acquisition of wild-type levels of NPQ in HL-grown *lhcx1* cells.

Different Quenching Capacities in LL- and HL-Treated Cells Reflect a Heterogenous Distribution of the LHCX Isoforms in Different Chloroplast Fractions

Previous studies have localized LHCX1 either in the FCP complexes (Lepetit et al., 2010; Schaller-Laudel et al., 2015) or in PSI (Grouneva et al., 2011). However, no information is available for the other LHCX isoforms. Therefore, we reinvestigated the localization of the

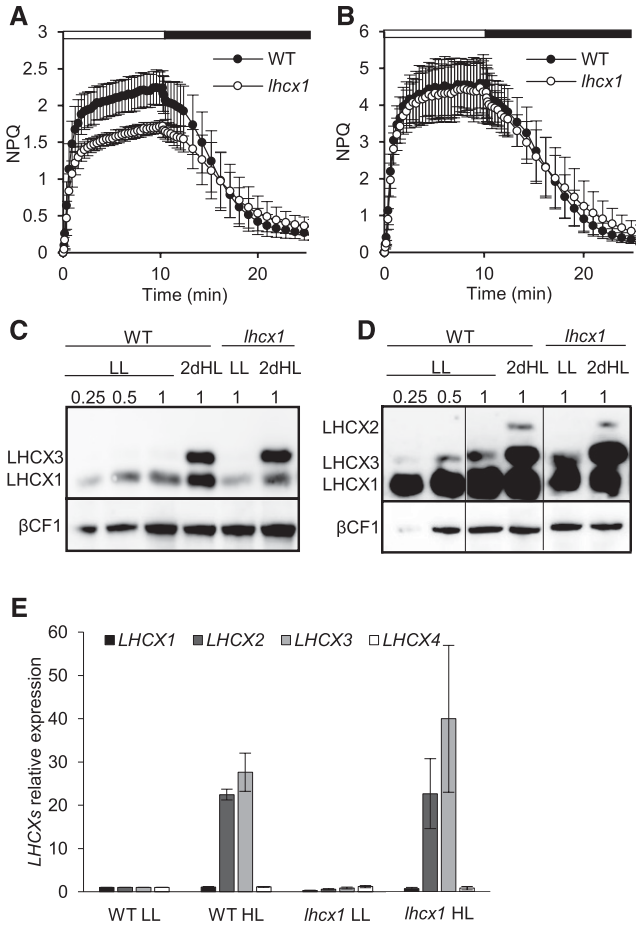

Figure 1. *LHCX1* knockdown cells recover their NPQ capacity during prolonged HL exposure. For all the experiments shown in this figure, cells were grown in 12-h-light/12-h-dark cycles either in LL (30 µmol photons m^{-2} s^{-1}) or in HL (500 µmol photons m^{-2} s^{-1}) for 2 d, following a shift from LL to HL. The samples were taken 2 h after the onset of light. A and B, NPQ capacity in *P. tricornutum* wild-type (WT; black circles) and *LHCX1* knockdown (*lhcx1*; white circles) cells grown under LL (A) or HL (B). Note that different vertical axes were used in A and B to better highlight the differences in NPQ between wild-type and *lhcx1* cells in LL and HL conditions. Error bars indicate SD of five independent experiments. C and D, Accumulation of the different *P. tricornutum* LHCX proteins in wild-type and *lhcx1* cells detected with an antibody against LHCSR/LHCX. Thirty micrograms from each protein extract was used, and the protein levels were quantified using a serial dilution of proteins from wild-type cells as a standard. The relative amount of protein loaded on the gel and the three detected *P. tricornutum* LHCX isoforms (Taddei et al., 2016) are indicated. βCF1 was used as a loading control. The longer exposure time of the membrane in D allowed us to detect the accumulation of the LHCX2 isoform in HL. The vertical lines indicate nonadjacent lanes taken from the same blot. E, Analysis of the relative transcript levels of *LHCX* by quantitative reverse transcription PCR in wild-type and *lhcx1* cells. Ribosomal protein small subunit 30S (Phatr3_J10847) was used as a reference gene, and for each LHCX, the values are relative to the wild-type level in LL. Error bars represent standard deviation of three technical replicates.

various LHCX proteins in the different photosynthetic complexes isolated by Suc density gradient centrifugation (Fig. 2A) from detergent-treated thylakoid membranes of *P. tricornutum*. Five distinct fractions were recovered from LL- and HL-treated wild-type and *lhcx1* strains (Fig. 2A). Using western-blot analysis, we identified them as free pigments, trimeric FCPs (i.e. the physiological antenna form in *P. tricornutum*; Lepetit et al., 2007; Joshi-Deo et al., 2010; Gardian et al., 2014), PSII monomers, PSI, and PSII dimers in accordance with earlier results obtained with clear native PAGE (Nagao et al., 2013). LHCX1, the only isoform strongly expressed in LL-treated cells, is ubiquitous, as it colocalizes with the FCP and PSI as well as with the PSII dimer fractions (Fig. 2B). As expected, samples isolated from *lhcx1* cells had a lower content of this protein. On the other hand, LHCX3, which is induced in HL-treated cells (Nymark et al., 2009; Bailleul et al., 2010; Lepetit et al., 2013, 2017; Taddei et al., 2016), seems to have a more specific localization, being found only in the FCP and PSI fractions (Fig. 2B). The LHCX2 isoform could not be detected by western-blot analysis, likely because of a lower level of accumulation as compared with LHCX3 in prolonged HL stress and a lower affinity of the antibody generated against the *Chlamydomonas reinhardtii* LHCSR3 for this isoform.

Prolonged Exposure to HL Induces a Change in the NPQ Quenching Site in *P. tricornutum* Cells

We employed picosecond spectrally resolved fluorescence measurements to analyze the quenching features in LL- and HL-treated wild-type and *lhcx1* cells. To discriminate between quenching in the antennas and PSII cores, we selectively excited different pigment populations. We excited fucoxanthin, which is found only in the FCP antenna complexes (Lepetit et al., 2010), with 540-nm light. Conversely, we used 400-nm light to excite chlorophyll *a* (Szabó et al., 2008; Chukhutsina et al., 2013), which is present in PSI and PSII cores and in the FCPs. Time-resolved fluorescence emission data were globally fitted to obtain the fluorescence lifetimes and the corresponding decay-associated spectra (DAS).

Global analysis of time-resolved fluorescence data was performed in wild-type and *lhcx1* lines in LL (Fig. 3) and HL (Fig. 4) excited at 400 and 540 nm, both in the quenched and unquenched states. We found that five components are required to accurately describe the fluorescence kinetics in LL (Fig. 3), and the results on wild-type cells upon excitation with 400-nm light are described in more detail below. The three components with the shortest lifetimes (14, 64, and 242 ps) mainly reflected excitation energy transfer (EET) from short-wavelength (high-energy) pigments to long-wavelength (low-energy) pigments. This downhill energy transfer could be recognized easily, because the corresponding DAS were positive on the short-wavelength side and negative on the long-wavelength side (van Stokkum et al., 2008). For example, the 14-ps DAS displayed a positive band at 675 nm and two negative bands at 690 and 717 nm.

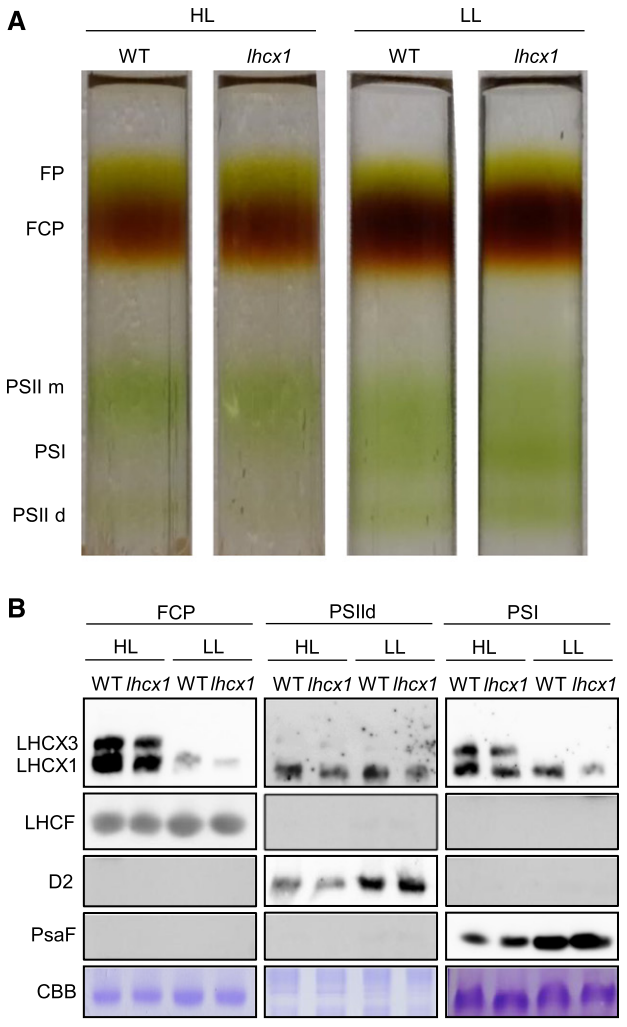

Figure 2. Localization of the LHCX isoforms in different chloroplast fractions. A, Suc density gradient fractionation of solubilized thylakoids from wild-type (WT) and *lhcx1* cells grown in LL and in HL for 2 d. FP, Free pigments; PSII m, PS II monomers; PSII d, PSII dimers. B, Western-blot analysis of the proteins extracted from the thylakoids and the FCP, PSII, and PSI fractions and detected with antibodies against LHCSR/LHCX, LHCF (antenna proteins), D2 (PSII), and PsaF (PSI). Gray images represent no signal detected after hybridization with the indicated antibodies. Samples were loaded at an equal chlorophyll amount (1 µg). CBB, Coomassie Brilliant Blue staining of the protein gels.

This reflected EET from chlorophyll (chlorophyll *a*) with fluorescence peaking around 675 nm (Chl_{675}) to Chl_{690} and Chl_{717} and represented mainly EET from FCPs to both photosystems, and possibly Lhcf15, a member of the Fucoxanthin Chlorophyll *a*/*c* Binding Protein family (Chukhutsina et al., 2014). Indeed, the peak position of Chl_{717} strongly resembled that of the red (long-wavelength) antennas composed of Lhcf15, which emit at 716 nm at 77 K (Herbstová et al., 2015, 2017). The assignment of this long-wavelength emission (to PSI or Lhcf15 or both) is discussed further in the next section. The second DAS represented a similar process occurring on a slower time scale (64 ps). The 242-ps (third) DAS reflected energy equilibration between Chl_{687} and Chl_{717} and, surprisingly, was 1 order of magnitude slower than that observed previously for FCPs of *Cyclotella meneghiniana* (Chukhutsina et al., 2014). This suggested that the red antennas are part of a large antenna system, in which it takes a relatively long time to reach some of the red-emitting species. The 894-ps DAS represented fluorescence decay processes in PSII and PSI emitting at 690 and 712 nm, respectively. The 4-ns DAS, emitting at 717 nm, again reflected relaxation of the red-most emitters of *P. tricornutum.* Figure 3 also shows the results for LL-treated wild-type cells in which NPQ has been induced. In this case, we found similar lifetimes (14 ps, 61 ps, 219 ps, 816 ps, and 4 ns) to those for unquenched cells (Fig. 3; Supplemental Table S2), but the DAS are different. The 14-ps spectrum was virtually identical for the quenched and unquenched samples, including the EET part to the long-wavelength pigments (Fig. 3). On the other hand, the 61- and 219-ps components showed strongly reduced EET to the long-wavelength band. As a result, the amplitude of the 4-ns DAS decreased substantially, corresponding to a decrease of the average fluorescence lifetime (Supplemental Table S3) and quenching of the fluorescence. We directly compared the steady-state fluorescence spectra, which have been reconstructed from the DAS as explained in "Materials and Methods." The resulting quenched and unquenched spectra for LL-treated wild-type cells are presented in Figure 5A. Both spectra were dominated by the red-shifted fluorescence band around 717 nm, but the spectrum corresponding to the NPQ state was substantially smaller. We also observed quenching of the 687-nm emission (Fig. 5, insets).

The same measurements were performed with a 540-nm excitation to preferentially excite the antenna (Fig. 3B), and the obtained DAS were very similar to those obtained upon 400-nm excitation (Fig. 3A). Also, the reconstructed steady-state spectra for quenched and unquenched cells (Fig. 5B) were very similar to those obtained with 400-nm excitation.

Time-resolved fluorescence measurements also were performed on LL-treated *lhcx1* cells, and the results for unquenched cells were very similar to those for wild-type cells (Fig. 3, C and D). The spectra for the quenched cells also were reminiscent of those of the wild-type cells. However, the amount of quenching was smaller, as can be seen for the reconstructed steady-state spectra in Figure 5, C and D. Moreover, quenching of the 687-nm emission was not present in the transgenic cells (Fig. 5, insets). It is important to note that the differences induced by NPQ cannot be compared directly with those obtained during fluorescence induction measurements, which were performed at room temperature (Fig. 1). Indeed, the fluorescence steady-state emission (Fig. 5) calculated at 77 K was dominated by the long-lived PSI fluorescence or other red-most-emitting species, at variance with fluorescence measured at room temperature.

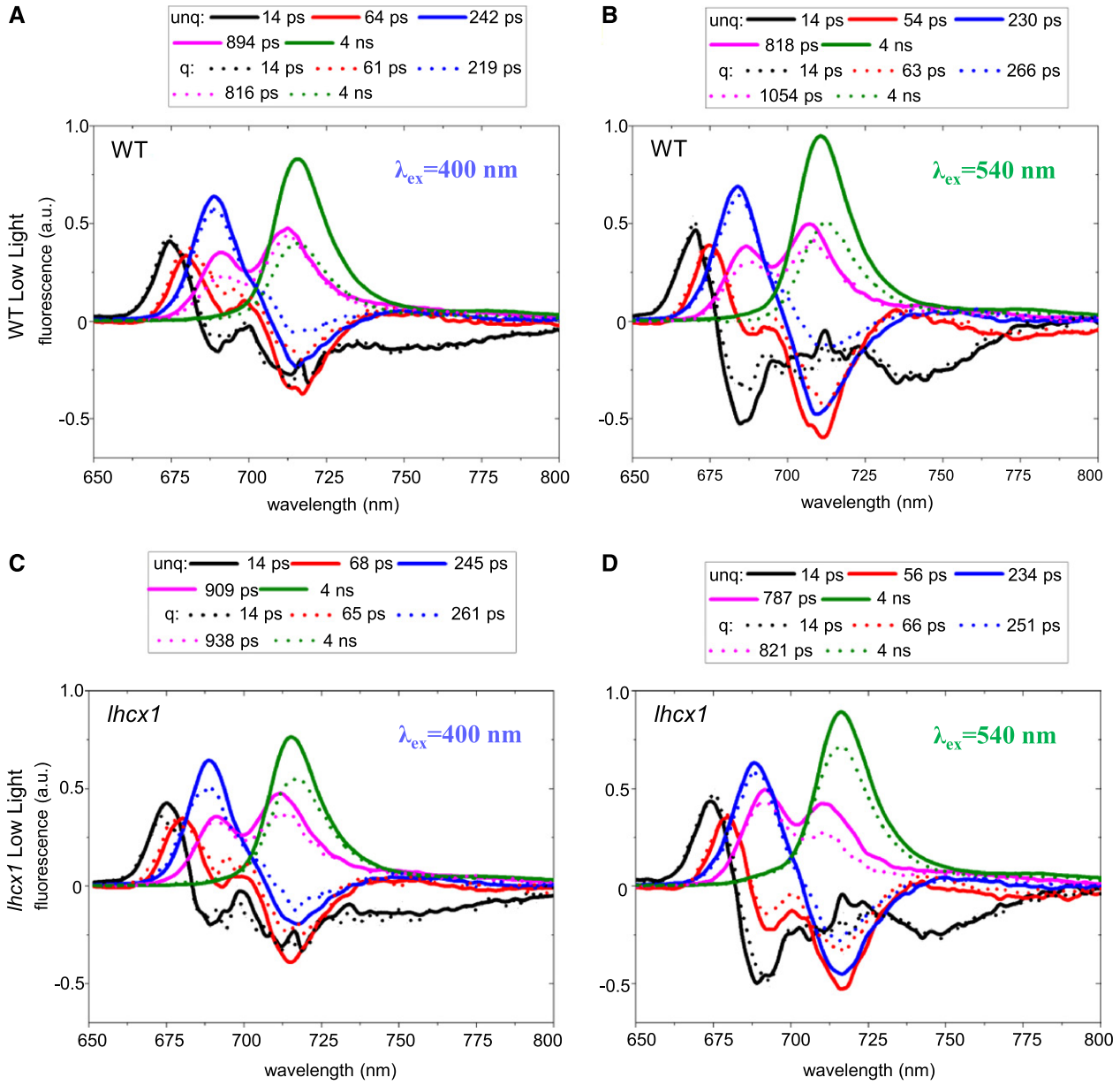

Figure 3. Time-resolved fluorescence analysis of *P. tricornutum* cells adapted to LL. A and B, DAS for wild-type (WT) cells upon a 400-nm excitation (A) and a 540-nm excitation (B) in unquenched (unq; solid lines) and quenched (q; dotted lines) states. C and D, DAS for *lhcx1* cells upon a 400-nm excitation (C) and a 540-nm excitation (D) in unquenched and quenched states. Measurements were performed at 77 K. DAS were calculated as explained in "Materials and Methods". a.u., arbitrary units.

Similar measurements were then performed on HL-treated cells (Fig. 4). Four decay components were sufficient to fit the data for both types of cells upon excitation with either 400 or 540 nm. In contrast to the results on LL-treated cells, there were substantial differences between the two excitation wavelengths that were clearly visible when comparing the reconstructed steady-state spectra (Fig. 5, E–H). Excitation of the antenna at 540 nm led to enhanced fluorescence quenching (Fig. 5F) as compared with 400-nm excitation (Fig. 5E), and this also was observed for the *lhcx1* cells (Fig. 5, G and H). Therefore, it can be concluded that, in HL-treated cells, a substantial portion of the quenching is localized in the FCPs. Earlier studies using time-resolved fluorescence (Miloslavina et al., 2009; Chukhutsina et al., 2014) identified two quenching sites in diatoms. The first one (Q1) was localized mainly in the antenna complexes that detach from the photosystems during quenching. The second one (Q2) was found in close proximity to the PSII core (Chukhutsina et al., 2014). In the frame of this model, our data suggest that Q1 quenching becomes more prominent in

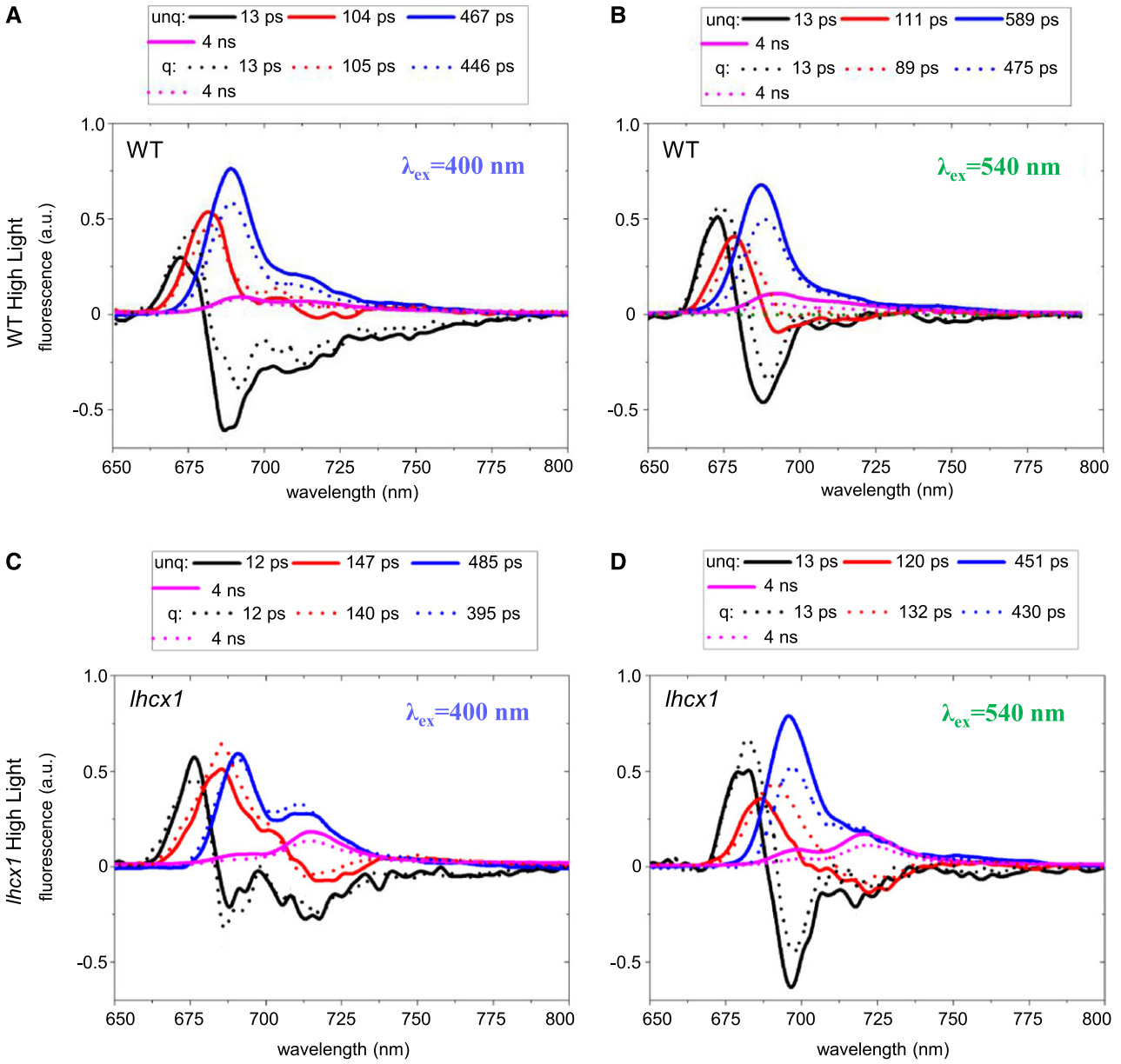

Figure 4. Time-resolved fluorescence analysis of *P. tricornutum* cells adapted to HL. A and B, DAS for wild-type (WT) cells upon a 400-nm excitation (A) and a 540-nm excitation (B) in unquenched (unq; solid lines) and quenched (q; dotted lines) states. C and D, DAS for *lhcx1* cells upon a 400-nm excitation (C) and a 540-nm excitation (D) in unquenched and quenched states. Measurements were performed at 77 K. DAS were calculated as explained in "Materials and Methods". a.u., arbitrary units.

P. tricornutum cells under HL conditions. Under LL conditions, this antenna-related quenching is not observed, and we conclude that the wild-type cells (and, to a far lesser extent, the *lhcx1* cells) develop NPQ mainly based on Q2-localized quenching.

Overall, the results of picosecond fluorescence decay spectroscopy and biochemistry suggest that LHCX1 is responsible for the large NPQ associated with the PSII core that is observed in LL. Hence, LHCX1 is mandatory for Q2. Conversely, the onset of the extra antenna-related NPQ observed in HL-exposed cells (Q1) should be due to the specific induction of other LHCX isoforms, such as LHCX3, detected predominantly in the antenna fraction.

Consequences of Antenna- and PSII Core-Localized Quenching on Light Acclimation of *P. tricornutum* Cells

Based on the conclusions from the picosecond fluorescence measurements (i.e. the preferential detection

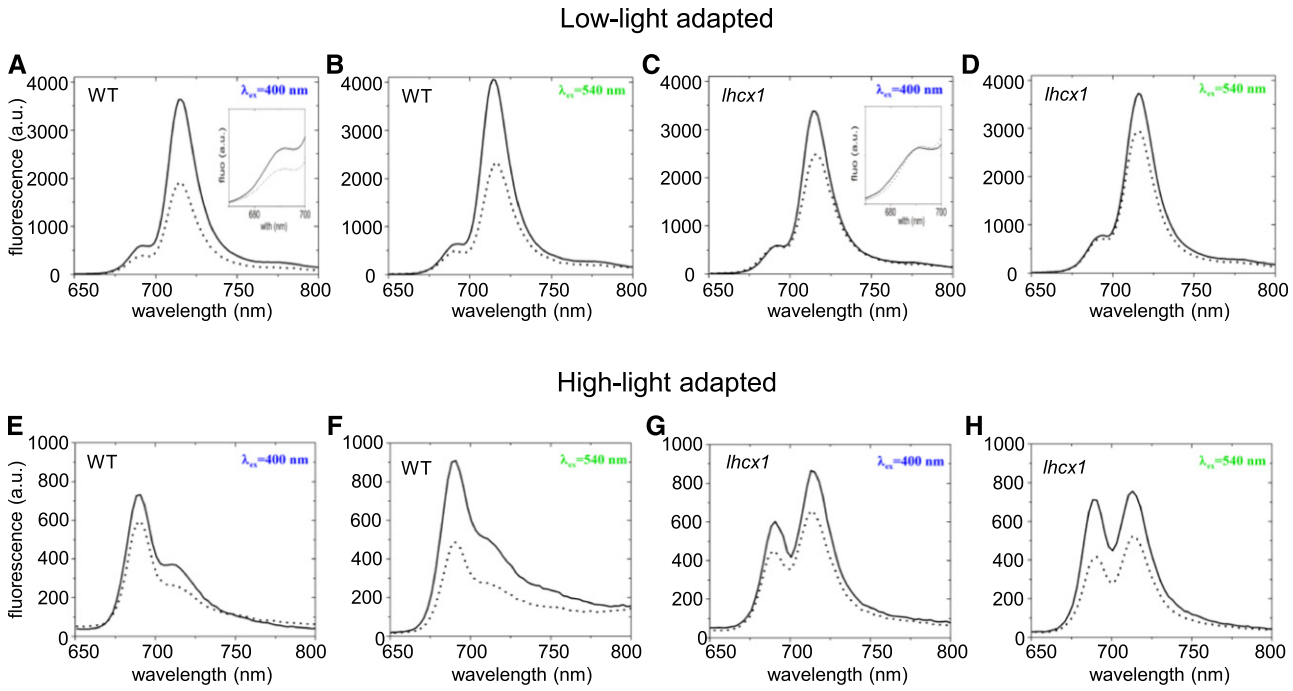

Figure 5. Reconstructed steady-state emission spectra in unquenched (solid lines) and quenched (dashed lines) states at 77 K of LL-adapted (top row) and HL-adapted (bottom row) cells. Excitation wavelengths and analyzed strains are indicated in every graph. Spectra were reconstructed as explained in "Materials and Methods". a.u., arbitrary units. Insets in A and C indicate comparison of reconstructed steady-state emission in the 670-700 nm spectral region.

of antenna [Q1] and PSII core [Q2] quenching in diatoms in HL and LL conditions, respectively), we tried to evaluate the relative efficiency of the two quenching mechanisms in protecting the photosynthetic apparatus from photodamage. To this aim, we compared the photosynthetic performances of wild-type and *lhcx1* cells grown either in LL, where the PSII core quenching is mostly active, or in HL, where antenna quenching becomes the prominent component of NPQ.

A shift from LL to HL for 2 d largely increased the photosynthetic activity of wild-type cells, indicating that the cells properly acclimate to the higher photon flux (Fig. 6A) and, therefore, sustain growth (Supplemental Fig. S2). In parallel to the increased photosynthesis, respiration also was enhanced (Supplemental Table S4), as expected because of the tight link between the two processes in diatoms (Bailleul et al., 2015). On the contrary, *lhcx1* cells were unable to increase their photosynthetic and respiratory capacities upon HL exposure for 2 d (Fig. 6B; Supplemental Table S4). By calculating PSII inactivation (either from changes in the F_v/F_m ratio or using the $1/F_o - 1/F_m$ parameter (see "Materials and Methods"; Campbell and Tyystjärvi, 2012), we observed a stronger photoinactivation in *lhcx1* knockdown cells compared with the wildtype (Supplemental Table S4) when exposed to HL. This also suggested that, despite the similar NPQ capacity of both cell lines in HL, *lhcx1* cells were more prone to photoinhibition than wild-type cells. This conclusion was supported by a biochemical analysis of the thylakoid main complexes using antibodies for the LHCX proteins, the PSII (D2) and PSI (PsaF) photosynthetic subunits (Fig. 6, C and D), and the ATPase complex subunit (βCF1). We found that both genotypes displayed reduced levels of PSII and PSI proteins upon exposure to HL for 2 d. Overall, these data confirm that *P. tricornutum* responds to increasing light intensities by reducing the number of reaction centers, a strategy known in diatoms and other microalgae as n-type photoacclimation (Falkowski and Owens, 1980). However, the effect on PSII was exacerbated in the *lhcx1* cells, suggesting that PSII was degraded specifically upon the high-light shift in *lhcx1* as a consequence of photoinhibition.

DISCUSSION

Our biochemical, spectroscopic, and physiological investigation suggests a model for photoprotection in *P. tricornutum* (Fig. 7) in which the differential accumulation of LHCX isoforms in different photosynthetic complexes modulates the efficiency of

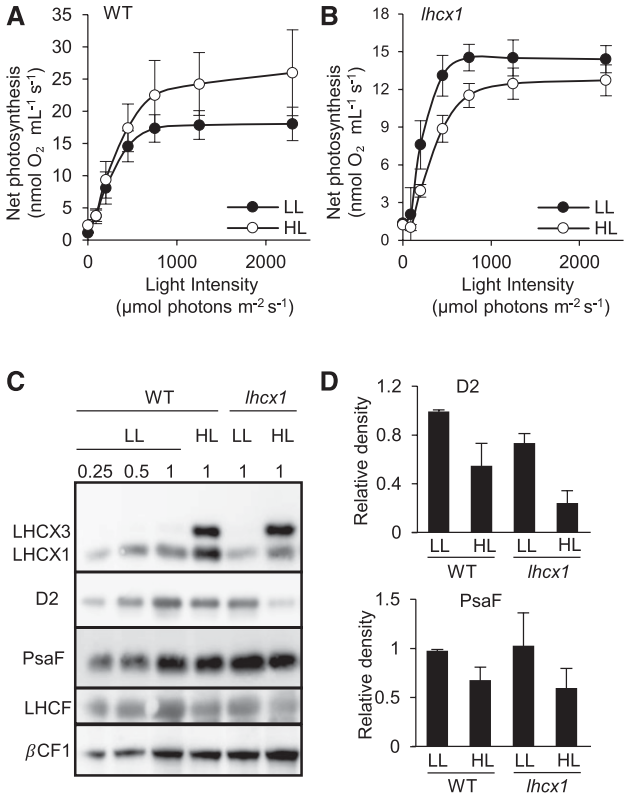

Figure 6. Physiological analysis of wild-type (WT) and *lhcx1* cells. A and B, Net photosynthesis calculated from the oxygen evolution rates minus oxygen consumption measured with a Clark electrode at different light intensities (0, 90, 200, 450, 750, and 2,300 µmol photons m^{-2} s^{-1}). Wild-type (A) and *lhcx1* (B) cells were grown in LL (30 µmol photons m^{-2} s^{-1}) or HL (500 µmol photons m^{-2} s^{-1}) for 2 d, following a shift from LL to HL. Error bars indicate the standard deviation of three biological replicates. C, Western-blot analysis of total protein extracts (30 µg) from cells grown in the same condition as in A and B. Antibodies against LHCSR/LHCX, LHCF, D2, PsaF, and βCF1 were used for protein detection. D, Densitometric analysis of D2 and PsaF obtained from independent western-blot analyses (three independent biological experiments) from wild-type and *lhcx1* cells grown as in C. Signals for D2 and PsaF were adjusted according to those of βCF1, used as a loading control, and normalized on the wild-type LL signal.

NPQ via different quenching mechanisms. We show that two main LHCX isoforms present in the light (LHCX1 and LHCX3; Taddei et al., 2016) are located in different regions in the photosynthetic complexes of this alga. While LHCX1 is distributed ubiquitously in PSI, PSII, and the FCPs, LHCX3 is associated only with the PSI and FCP complexes. Moreover, LHCX1 and LHCX3 are differentially expressed depending on the light regime. LHCX1 is the predominant isoform in LL, while LHCX1 and LHCX3 accumulate in HL-exposed cells. We suggest that, in LL-acclimated cells, LHCX1 would provide a constitutive NPQ capacity localized mainly near the PSII core (Q2; Miloslavina et al., 2009; Chukhutsina et al., 2014), where LHCX1 is found (Fig. 7). The existence of a link between this quenching and LHCX1 is supported by the finding that the NPQ amplitude is reduced when the content of LHCX1 is diminished (e.g. in the *lhcx1* knockdown line, in the Pt4 ecotype, and also in wild-type cells at the end of the day; Bailleul et al., 2010). In addition to this basal quenching process, an additional quenching is observed upon HL exposure for a few days (Lepetit et al., 2013, 2017). This quenching is localized mostly in the FCPs and, therefore, corresponds to the previously identified Q1 type of quenching (Miloslavina et al., 2009; Chukhutsina et al., 2014). In the antenna, Q1 would benefit from the additional presence of the HL-inducible LHCX3 isoform (Fig. 7), and possibly the LHCX2 isoform in this process, which also accumulates to some extent under HL stress (Taddei et al., 2016; Lepetit et al., 2017).

Our physiological data also allowed us to assess the relative efficiency of the two LHCX-related NPQ mechanisms. While both the wild-type and *lhcx1* lines have comparable NPQ capacity in HL, *lhcx1* cells are more prone to photoinhibition. However, antenna quenching, Q1, is prominent in cells with a deregulated LHCX1 expression, while Q2 quenching (PSII core quenching) dominates in the wild type. Overall, this observation suggests that PSII core quenching is more efficient in protecting diatoms against photoinhibition of PSII, as hypothesized recently (Kuzminov and Gorbunov, 2016; Giovagnetti and Ruban, 2017). In the frame of this model, the differences in NPQ (Fig. 1) and photosynthesis (Fig. 6) between wild-type and *lhcx1* cells in LL versus HL conditions can be explained based on the presence of distinct complexes that are differentially quenched by members of the LHCX family.

Consistent with the above scenario, previous studies have revealed a fine-tuning of qE based on changes in the amount/localization of the qE protein effectors in other photosynthetic organisms. In plants, Bergantino et al. (2003) proposed that PsbS could trigger different types of NPQ via its association with either the PSII core or the LHCII antenna complexes. This would occur via a hypothesized protein monomerization, which was recently observed experimentally in vitro (Fan et al., 2015). Consistent with this idea, a fast-developing NPQ is lost in the NoM mutant lacking PSII core-bound monomeric LHCs, while the slow-developing quenching was unaffected (Dall'Osto et al., 2017). In green algae, differential binding of LHCSR3 to PSI and PSII has been reported and related to changes in NPQ (Allorent et al., 2013). Recently, Pinnola et al. (2015) also showed that PSI-bound LHCSR1 induces NPQ in this complex in the moss *Physcomitrella patens*. Our finding that LHCX3 is bound to PSI is consistent with the occurrence of a similar quenching process in diatoms as well. However, testing this possibility is difficult in diatoms due to the peculiar nature of the long-wavelength fluorescence band around 717 to 720 nm, which is seen in *P. tricornutum* cells, especially in LL-treated cells.

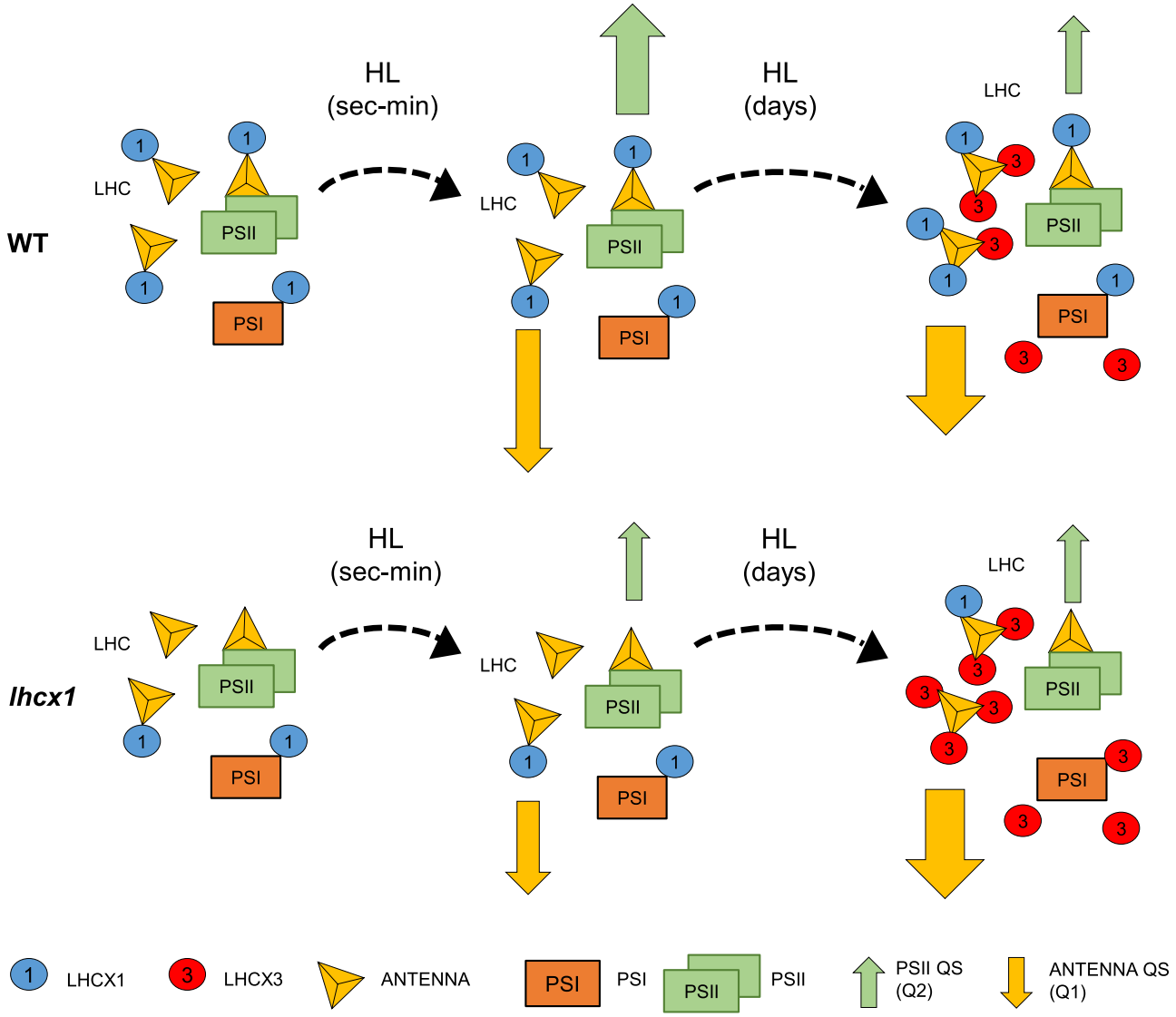

Figure 7. Model for NPQ in *P. tricornutum* wild-type (WT) and *lhcx1* cells adapted to LL and after short and long exposures to HL. In LL-grown wild-type cells experiencing a short HL treatment (from seconds to minutes), the major quenching site is close to the reaction center (Q2). *lhcx1* cells show a reduced quenching capacity because of the reduced content of LHCX1, the highly expressed isoform in LL. After prolonged HL treatment (days), the quenching sites are mainly in the FCP red-shifted antenna (Q1). The *lhcx1* line recovers its NPQ capacity. Because of the similar quenching capacity in wild-type and *lhcx1* cells, this quenching could be related to LHCX3, which is highly induced in HL and is detected in the FCP fraction.

In plants and green algae, PSII and PSI fluorescence emission can be distinguished easily by their spectral features and lifetimes, with PSI emitting at longer wavelengths with a shorter lifetime. In diatoms, the 717- to 720-nm band has been attributed to emission by a PSII-associated red-shifted antenna (Herbstová et al., 2015, 2017). In our global analysis of wild-type cells excited at 400 nm, we observed three DAS that show EET toward the long-wavelength pigments. The fastest component of 14 ps is characteristic for EET in PSI and is observed for PSI from the plant Arabidopsis (*Arabidopsis thaliana*; Wientjes et al., 2011; Tian et al., 2017) and the green alga *C. reinhardtii* (Ünlü et al., 2016; Wlodarczyk et al., 2016). The observed time constants for the major part of the transfer range from 5 to 11 ps in Arabidopsis to 7 to 29 ps in *C. reinhardtii*, which is similar to the 14 ps observed for LL-treated wild-type unquenched cells. The other components reflecting EET to the long-wavelength pigments are far slower (64 and 242 ps) than usually observed for PSI, and we ascribe them to transfer to Lhcf15 proteins, which are known to emit at 716 nm at 77 K (Herbstová et al., 2015, 2017). It is also worthwhile to mention that no nanosecond component with PSI character-

istics has been observed for diatoms (Chukhutsina et al., 2014), in contrast to what has been reported for native membranes of higher plants or cyanobacteria, where DAS with 2- and 7.4-ns lifetimes represent slow PSI trapping from red pigments (van der Weij-de Wit et al., 2011; Chukhutsina et al., 2015). Interestingly, when NPQ is induced in the LL-treated wild-type cells, the fastest DAS remain entirely unchanged as well as the 14-ps lifetime. This finding suggests that LHCX1 does not induce quenching of PSI but rather induces quenching on the red-shifted antennas of PSII. Consistent with this, transfer to the long-wavelength pigments of Lhcf15 is reduced considerably, leading to substantial quenching of their fluorescence. The results obtained for the 540-nm excitation also are consistent with this picture, and the same is true for the results on LL-treated *lhcx1* cells. When the cells are grown in HL, the long-wavelength fluorescence is strongly reduced. However, upon induction of NPQ, the long-wavelength band also is quenched. Again, no clear difference is observed in the fastest DAS, which corresponds to EET to the long-wavelength band, while quenching is due mainly to the reduction of the 4-ns component. These findings suggest that, like LHCX1, LHCX3 does not induce NPQ in PSI but rather in the red-shifted antennas of PSII, although the possibility of quenching in PSI cannot be ruled out unambiguously.

Overall, we propose that active regulation of the two forms of quenching by different LHCX isoforms provides a rationale for the existence of several isoforms of these qE effectors, their number being, on average, larger than that found in all the other algal species studied thus far (Taddei et al., 2016; Mock et al., 2017). Multiple regulation of the LHCX family members by nutrient starvation (Taddei et al., 2016) and other stresses (e.g. light fluctuation [Lepetit et al., 2017] and prolonged darkness [Taddei et al., 2016]) would provide additional degrees of flexibility in controlling responses to environmental changes, as required for efficient acclimation to the continuous changes of the ocean environment.

MATERIALS AND METHODS

Strains and Culture Conditions

Axenic *Phaeodactylum tricornutum* (Pt1 8.6, CCMP2561) wildtype and the *lhcx1* knockdown (Bailleul et al., 2010) strain were grown in f/2 medium at 19°C in a 12-h-light/12-h-dark photoperiod. Cells were first acclimated to 30 µmol photons m^{-2} s^{-1} (LL) and then shifted to 500 µmol photons m^{-2} s^{-1} (HL) white light for 2 d. Cells were collected during the exponential phase of growth.

Oxygen Evolution and Consumption

Rates of oxygen evolution and consumption were measured with a Clark electrode (Hansatech) at different light intensities (0, 90, 200, 450, 750, and 2,300 µmol photons m^{-2} s^{-1}), and the measurement was performed when the signal was stable. Illumination was maintained for 2 min at every intensity to attain steady-state oxygen evolution while avoiding an excessive illumination that could lead to photoinhibition. Net photosynthesis was calculated as light-driven oxygen evolution minus dark respiration.

Pigment Analysis

Pigment extraction was performed on cells grown either in LL or HL for 2 d. Cells were irradiated for 10 min with strong HL before being collected by quick filtration. Pigments were extracted on ice using 96% (v/v) ethanol, buffered with Na_2CO_3 in the dark for 30 min, and centrifuged. The supernatant was loaded in a high-performance liquid chromatograph (Thermo-Fisher) with a detector diode array to analyze the visible region with a C18 Spherisorb column (7.3 × 30 mm) using an aqueous mixture of acetonitrile:methanol:0.1 M Tris-HCl buffer (pH 8; 72:8:3, v/v/v; buffer A) and a methanol:hexane mixture (4:1, v/v; buffer B). The runs were done at a flux of 1.5 mL, starting with 100% buffer A: 0 to 5 min, 97% A; 5 to 17 min, gradient to 80% A; 17 to 18 min, to 100% buffer B; and 18 to 23 min, 100% B. Pigments are distinguishable by the retention time and by the absorption spectrum. The deepoxidation state was calculated as (Z+1/2A)/(Z+A+V) or as (DT)/(DT+DD) [Ruban et al., 2004; Bonente et al., 2011].

Isolation of Pigment-Protein Complexes

Thylakoid membrane isolation and solubilization were conducted following the protocol by Lepetit et al. (2007). Equal amounts of isolated thylakoids, corresponding to 0.5 to 1 mg of total chlorophyll, were solubilized with *n*-dodecyl *β*-D-maltoside (DM; Carl Roth) at detergent:chlorophyll ratios of 30 corresponding to 3% (w/v) DM. The solubilized thylakoids were applied immediately to linear Suc gradients (from 0 to 0.6 M Suc [w/v] in isolation medium B complemented with 0.03% DM). Samples were centrifuged for 17 h at 110,000*g* using a swing-out rotor. After the separation, Suc gradient bands were harvested with a syringe and stored for further characterization at −20°C.

Expression Analyses

Total RNA were extracted and analyzed by quantitative reverse transcription PCR as described (Taddei et al., 2016). Total proteins were extracted and analyzed by western blot as described previously (Bailleul et al., 2010). Proteins from photosynthetic complexes were analyzed by charging equal amounts of chlorophyll (1 µg), quantified according to Lohr and Wilhelm (2001). Proteins were detected by specific antibodies: anti-LHCSR (dilution 1:5,000; a gift of G. Peers, University of California), anti-D2 (dilution 1:10,000; a gift of J.-D. Rochaix, University of Geneva), anti-PsaF and anti-*β*CF1 for the chloroplastic ATPase (dilution 1:1,000 and 1:10,000, respectively; gifts of F.-A. Wollman, Institut de Biologie Physico-Chimique), and anti-LHCF1-11 (dilution 1:2,000; a gift of C. Büchel, Institut für Molekulare Biowissenschaften Universität Frankfurt). Densitometry measurements of each protein signal were performed using ImageJ (Schneider et al., 2012). Protein signals in the linear range of detection were adjusted for loading according to the corresponding *β*CF1 signal, and values were normalized to the value of the wild type in the LL condition.

Room Temperature Chlorophyll Fluorescence Measurements

The kinetics of chlorophyll fluorescence yields at room temperature were measured using a fluorescence CCD camera recorder (Speezen1; JBeamBio; Johnson et al., 2009) on cells at 1×10^6 to 2×10^6 cells mL^{-1}. Before the measurements, all samples were adapted to ambient, dim light for 15 min at 18°C to relax the reaction centers. The F_v/F_m ratio was calculated as $(F_m - F_o)/F_m$, where F_m and F_o are the maximum and minimum fluorescence emission levels during a saturating pulse and in the dark, respectively. NPQ was calculated as $(F_m - F_m')/F_m'$ (Bilger and Björkman, 1990), where F_m' is the maximum fluorescence emission level in cells exposed to actinic light, measured with the saturating pulse of light. The maximal NPQ response was measured upon exposure for 10 min to saturating 950 µmol m^{-2} s^{-1} green light. Photoinactivation was determined as $1/F_o - 1/F_m$ (Park et al., 1995; He and Chow, 2003; Wu et al., 2011; Campbell and Tyystjärvi, 2012). Here, the value $1/F_o - 1/F_m$ of LL-acclimated or 2 d of HL-acclimated cells was taken before starting a short HL treatment (950 µmol m^{-2} s^{-1}) and was set to 100%. The percentage of functional PSII was estimated by calculating $1/F_o - 1/F_m$ after the 10-min HL treatment and 15 min of darkness.

Low-Temperature Time-Resolved Fluorescence Emission Spectra Measurements Using a Streak Camera

Time-resolved emission spectra were recorded using a synchroscan streak camera system as described (van Oort et al., 2009). An excitation wavelength of 540 nm was used to preferentially excite fucoxanthin in the antenna, while 400 nm was used to preferentially excite chlorophyll *a* in the antenna and the cores. All samples were measured in two different states: the original (unquenched) state (10 min of dark adaptation) and the quenched state (~10 min of preillumination with white light at ~400 µmol photons m^{-2} s^{-1}). The laser power was 40 to 60 µW, the time window was 2 ns, the spot size was 100 µm, and the repetition rate was 250 kHz. An average of 100 images, all measured for 10 s, was used to achieve a high signal-to-noise ratio. Before analysis, the images were corrected for background signal and detector sensitivity and sliced into traces of 5 nm. The streak camera images were analyzed as described previously (Chukhutsina et al., 2013) with a singular-value-decomposition algorithm (van Stokkum et al., 2004). In short, the total data set was fitted with the function f(t, λ):

where DAS are the wavelength-dependent amplitude factors associated with decay component i having a decay lifetime τ_i (van Stokkum et al., 2004). The number of significant decay components was determined by the singular-value-decomposition algorithm analysis of the data and was five for LL and four for HL. A Gaussian-shaped instrument response function [i(t)] was used as input for the analysis with the width as a free-fitting parameter. The full width at half-maximum values of this function, obtained from the fitting procedure, were in the range of 28 ± 2 ps. The slowest component was always fixed to 4 ns. Due to the limited time window of our setup, it was not possible to resolve this component in an accurate way, but for the analysis presented, the exact value is not important. When we add all five DAS for a specific sample and excitation wavelength, then we obtain the fluorescence spectrum immediately after excitation (t = 0) before any spectral evolution has taken place in the corresponding wavelength region (unless some processes are too fast to be detected). This can be derived by filling in t = 0 in the equation above, which leads to $\exp(-t/\tau_i) = 1$ for all values of *i*. The resulting t = 0 spectra (before the fluorescence decays set in) do not depend on the state of the cells (unquenched/quenched), as expected. For comparison of fluorescence emission in quenched and unquenched states (Fig. 5), the total fluorescence spectra at t = 0 are normalized to their maximum, while the DAS are scaled accordingly. These scaled DAS also were used to reconstruct the steady-state fluorescence spectra by multiplying the individual, scaled DAS with their corresponding lifetime and taking their weighted sum.

Accession Numbers

Sequence data from this article can be found on the *P. tricornutum* genome browser (annotation Phatr3) on the Ensembl portal (http://protists.ensembl.org/Phaeodactylum_tricornutum/Info/Index) under the following identifier numbers: LHCX1, Phatr3_J27278; LHCX2, Phatr3_EG02404; LHCX3, Phatr3_J44733; and LHCX4, Phatr3_J38720.

Supplemental Data

The following supplemental materials are available.

Supplemental Figure S1. Representative fluorescence traces used to calculate NPQ values in Figure 1.

Supplemental Figure S2. Growth rate analysis of wild-type and LHCX1 knockdown (*lhcx1*) lines after a low light-to-high light shift.

Supplemental Table S1. Pigment composition of *P. tricornutum* wild-type and *lhcx1* knockdown lines grown either in low or high light for 2 d.

Supplemental Table S2. Results of global fitting of the streak camera data upon 400- and 540-nm excitation in unquenched and quenched states.

Supplemental Table S3. Calculated averaged lifetimes at characteristic wavelengths in *P. tricornutum* wild-type and *lhcx1* lines grown in low light or high light.

Supplemental Table S4. Photosystem II efficiency in wild-type and *lhcx1* lines.

Received April 24, 2018; accepted May 4, 2018; published May 17, 2018.

LITERATURE CITED

Alboresi A, Gerotto C, Giacometti GM, Bassi R, Morosinotto T (2010) Physcomitrella patens mutants affected on heat dissipation clarify the evolution of photoprotection mechanisms upon land colonization. Proc Natl Acad Sci USA **107**: 11128–11133

Alipanah L, Rohloff J, Winge P, Bones AM, Brembu T (2015) Whole-cell response to nitrogen deprivation in the diatom *Phaeodactylum tricornutum*. J Exp Bot **66**: 6281–6296

Allen AE, Laroche J, Maheswari U, Lommer M, Schauer N, Lopez PJ, Finazzi G, Fernie AR, Bowler C (2008) Whole-cell response of the pennate diatom *Phaeodactylum tricornutum* to iron starvation. Proc Natl Acad Sci USA **105**: 10438–10443

Allen AE, Dupont CL, Oborník M, Horák A, Nunes-Nesi A, McCrow JP, Zheng H, Johnson DA, Hu H, Fernie AR, (2011) Evolution and metabolic significance of the urea cycle in photosynthetic diatoms. Nature **473**: 203–207

Allorent G, Tokutsu R, Roach T, Peers G, Cardol P, Girard-Bascou J, Seigneurin-Berny D, Petroutsos D, Kuntz M, Breyton C, (2013) A dual strategy to cope with high light in *Chlamydomonas reinhardtii*. Plant Cell **25**: 545–557

Bailleul B, Rogato A, de Martino A, Coesel S, Cardol P, Bowler C, Falciatore A, Finazzi G (2010) An atypical member of the light-harvesting complex stress-related protein family modulates diatom responses to light. Proc Natl Acad Sci USA **107**: 18214–18219

Bailleul B, Berne N, Murik O, Petroutsos D, Prihoda J, Tanaka A, Villanova V, Bligny R, Flori S, Falconet D, (2015) Energetic coupling between plastids and mitochondria drives CO2 assimilation in diatoms. Nature **524**: 366–369

Ballottari M, Truong TB, De Re E, Erickson E, Stella GR, Fleming GR, Bassi R, Niyogi KK (2016) Identification of pH-sensing sites in the light harvesting complex stress-related 3 protein essential for triggering non-photochemical quenching in *Chlamydomonas reinhardtii*. J Biol Chem **291**: 7334–7346

Bergantino E, Segalla A, Brunetta A, Teardo E, Rigoni F, Giacometti GM, Szabò I (2003) Light- and pH-dependent structural changes in the PsbS subunit of photosystem II. Proc Natl Acad Sci USA **100**: 15265–15270

Bilger W, Björkman O (1990) Role of the xanthophyll cycle in photoprotection elucidated by measurements of light-induced absorbance changes, fluorescence and photosynthesis in leaves of *Hedera canariensis*. Photosynth Res **25**: 173–185

Bonente G, Formighieri C, Mantelli M, Catalanotti C, Giuliano G, Morosinotto T, Bassi R (2011) Mutagenesis and phenotypic selection as a strategy toward domestication of *Chlamydomonas reinhardtii* strains for improved performance in photobioreactors. Photosynth Res **108**: 107–120

Campbell DA, Tyystjärvi E (2012) Parameterization of photosystem II photoinactivation and repair. Biochim Biophys Acta **1817**: 258–265

Chukhutsina VU, Büchel C, van Amerongen H (2013) Variations in the first steps of photosynthesis for the diatom *Cyclotella meneghiniana* grown under different light conditions. Biochim Biophys Acta **1827**: 10–18

Chukhutsina VU, Büchel C, van Amerongen H (2014) Disentangling two non-photochemical quenching processes in *Cyclotella meneghiniana* by spectrally-resolved picosecond fluorescence at 77K. Biochim Biophys Acta **1837**: 899–907

Chukhutsina V, Bersanini L, Aro EM, van Amerongen H (2015) Cyanobacterial light-harvesting phycobilisomes uncouple from photosystem I during dark-to-light transitions. Sci Rep **5**: 14193

Dall'Osto L, Cazzaniga S, Bressan M, Paleček D, Židek K, Niyogi KK, Fleming GR, Zigmantas D, Bassi R (2017) Two mechanisms for dissipation of excess light in monomeric and trimeric light-harvesting complexes. Nat Plants **3**: 17033

de Vargas C, Audic S, Henry N, Decelle J, Mahé F, Logares R, Lara E, Berney C, Le Bescot N, Probert I, (2015) Ocean plankton: eukaryotic plankton diversity in the sunlit ocean. Science **348**: 1261605

Eberhard S, Finazzi G, Wollman FA (2008) The dynamics of photosynthesis. Annu Rev Genet **42**: 463–515

Falkowski PG, Owens TG (1980) Light-shade adaptation: two strategies in marine phytoplankton. Plant Physiol **66**: 592–595

Fan M, Li M, Liu Z, Cao P, Pan X, Zhang H, Zhao X, Zhang J, Chang W (2015) Crystal structures of the PsbS protein essential for photoprotection in plants. Nat Struct Mol Biol **22**: 729–735

Gardian Z, Litvín R, Bína D, Vácha F (2014) Supramolecular organization of fucoxanthin-chlorophyll proteins in centric and pennate diatoms. Photosynth Res **121**: 79–86

Ghazaryan A, Akhtar P, Garab G, Lambrev PH, Büchel C (2016) Involvement of the Lhcx protein Fcp6 of the diatom *Cyclotella meneghiniana* in the macroorganisation and structural flexibility of thylakoid membranes. Biochim Biophys Acta **1857**: 1373–1379

Giovagnetti V, Ruban AV (2017) Detachment of the fucoxanthin chlorophyll a/c binding protein (FCP) antenna is not involved in the acclimative regulation of photoprotection in the pennate diatom *Phaeodactylum tricornutum*. Biochim Biophys Acta **1858**: 218–230

Grouneva I, Rokka A, Aro EM (2011) The thylakoid membrane proteome of two marine diatoms outlines both diatom-specific and species-specific features of the photosynthetic machinery. J Proteome Res **10**: 5338–5353

He J, Chow WS (2003) The rate coefficient of repair of photosystem II after photoinactivation. Physiol Plant **118**: 297–304

Herbstová M, Bína D, Koník P, Gardian Z, Vácha F, Litvín R (2015) Molecular basis of chromatic adaptation in pennate diatom *Phaeodactylum tricornutum*. Biochim Biophys Acta **1847**: 534–543

Herbstová M, Bína D, Kaňa R, Vácha F, Litvín R (2017) Red-light phenotype in a marine diatom involves a specialized oligomeric red-shifted antenna and altered cell morphology. Sci Rep **7**: 11976

Horton P, Ruban AV, Walters RG (1996) Regulation of light harvesting in green plants. Annu Rev Plant Physiol Plant Mol Biol **47**: 655–684

Johnson X, Vandystadt G, Bujaldon S, Wollman FA, Dubois R, Roussel P, Alric J, Béal D (2009) A new setup for in vivo fluorescence imaging of photosynthetic activity. Photosynth Res **102**: 85–93

Joshi-Deo J, Schmidt M, Gruber A, Weisheit W, Mittag M, Kroth PG, Büchel C (2010) Characterization of a trimeric light-harvesting complex in the diatom *Phaeodactylum tricornutum* built of FcpA and FcpE proteins. J Exp Bot **61**: 3079–3087

Kuzminov FI, Gorbunov MY (2016) Energy dissipation pathways in photosystem 2 of the diatom, *Phaeodactylum tricornutum*, under high-light conditions. Photosynth Res **127**: 219–235

Lepetit B, Volke D, Szabó M, Hoffmann R, Garab G, Wilhelm C, Goss R (2007) Spectroscopic and molecular characterization of the oligomeric antenna of the diatom *Phaeodactylum tricornutum*. Biochemistry **46**: 9813–9822

Lepetit B, Volke D, Gilbert M, Wilhelm C, Goss R (2010) Evidence for the existence of one antenna-associated, lipid-dissolved and two protein-bound pools of diadinoxanthin cycle pigments in diatoms. Plant Physiol **154**: 1905–1920

Lepetit B, Sturm S, Rogato A, Gruber A, Sachse M, Falciatore A, Kroth PG, Lavaud J (2013) High light acclimation in the secondary plastids containing diatom *Phaeodactylum tricornutum* is triggered by the redox state of the plastoquinone pool. Plant Physiol **161**: 853–865

Lepetit B, Gélin G, Lepetit M, Sturm S, Vugrinec S, Rogato A, Kroth PG, Falciatore A, Lavaud J (2017) The diatom *Phaeodactylum tricornutum* adjusts nonphotochemical fluorescence quenching capacity in response to dynamic light via fine-tuned Lhcx and xanthophyll cycle pigment synthesis. New Phytol **214**: 205–218

Lohr M, Wilhelm C (1999) Algae displaying the diadinoxanthin cycle also possess the violaxanthin cycle. Proc Natl Acad Sci USA **96**: 8784–8789

Lohr M, Wilhelm C (2001) Xanthophyll synthesis in diatoms: quantification of putative intermediates and comparison of pigment conversion kinetics with rate constants derived from a model. Planta **212**: 382–391

Malviya S, Scalco E, Audic S, Vincent F, Veluchamy A, Poulain J, Wincker P, Iudicone D, de Vargas C, Bittner L, (2016) Insights into global diatom distribution and diversity in the world's ocean. Proc Natl Acad Sci USA **113**: E1516–E1525

Marchetti A, Schruth DM, Durkin CA, Parker MS, Kodner RB, Berthiaume CT, Morales R, Allen AE, Armbrust EV (2012) Comparative metatranscriptomics identifies molecular bases for the physiological responses of phytoplankton to varying iron availability. Proc Natl Acad Sci USA **109**: E317–E325

Matthijs M, Fabris M, Broos S, Vyverman W, Goossens A (2016) Profiling of the early nitrogen stress response in the diatom *Phaeodactylum tricornutum* reveals a novel family of RING-domain transcription factors. Plant Physiol **170**: 489–498

McQuaid JB, Kustka AB, Oborník M, Horák A, McCrow JP, Karas BJ, Zheng H, Kindeberg T, Andersson AJ, Barbeau KA, (2018) Carbonate-sensitive phytotransferrin controls high-affinity iron uptake in diatoms. Nature **555**: 534–537

Miloslavina Y, Grouneva I, Lambrev PH, Lepetit B, Goss R, Wilhelm C, Holzwarth AR (2009) Ultrafast fluorescence study on the location and mechanism of non-photochemical quenching in diatoms. Biochim Biophys Acta **1787**: 1189–1197

Mock T, Otillar RP, Strauss J, McMullan M, Paajanen P, Schmutz J, Salamov A, Sanges R, Toseland A, Ward BJ, (2017) Evolutionary genomics of the cold-adapted diatom *Fragilariopsis cylindrus*. Nature **541**: 536–540

Morrissey J, Sutak R, Paz-Yepes J, Tanaka A, Moustafa A, Veluchamy A, Thomas Y, Botebol H, Bouget FY, McQuaid JB, (2015) A novel protein, ubiquitous in marine phytoplankton, concentrates iron at the cell surface and facilitates uptake. Curr Biol **25**: 364–371

Müller P, Li XP, Niyogi KK (2001) Non-photochemical quenching: a response to excess light energy. Plant Physiol **125**: 1558–1566

Nagao R, Takahashi S, Suzuki T, Dohmae N, Nakazato K, Tomo T (2013) Comparison of oligomeric states and polypeptide compositions of fucoxanthin chlorophyll a/c-binding protein complexes among various diatom species. Photosynth Res **117**: 281–288

Nymark M, Valle KC, Brembu T, Hancke K, Winge P, Andresen K, Johnsen G, Bones AM (2009) An integrated analysis of molecular acclimation to high light in the marine diatom *Phaeodactylum tricornutum*. PLoS ONE **4**: e7743

Park YI, Chow W, Anderson J (1995) Light inactivation of functional photosystem II in leaves of peas grown in moderate light depends on photon exposure. Planta **196**: 401–411

Peers G, Truong TB, Ostendorf E, Busch A, Elrad D, Grossman AR, Hippler M, Niyogi KK (2009) An ancient light-harvesting protein is critical for the regulation of algal photosynthesis. Nature **462**: 518–521

Pinnola A, Cazzaniga S, Alboresi A, Nevo R, Levin-Zaidman S, Reich Z, Bassi R (2015) Light-harvesting complex stress-related proteins catalyze excess energy dissipation in both photosystems of *Physcomitrella patens*. Plant Cell **27**: 3213–3227

Ruban A, Lavaud J, Rousseau B, Guglielmi G, Horton P, Etienne AL (2004) The super-excess energy dissipation in diatom algae: comparative analysis with higher plants. Photosynth Res **82**: 165–175

Schaller-Laudel S, Volke D, Redlich M, Kansy M, Hoffmann R, Wilhelm C, Goss R (2015) The diadinoxanthin diatoxanthin cycle induces structural rearrangements of the isolated FCP antenna complexes of the pennate diatom *Phaeodactylum tricornutum*. Plant Physiol Biochem **96**: 364–376

Schneider CA, Rasband WS, Eliceiri KW (2012) NIH Image to ImageJ: 25 years of image analysis. Nat Methods **9**: 671–675

Smetacek V (1999) Diatoms and the ocean carbon cycle. Protist **150**: 25–32

Szabó M, Lepetit B, Goss R, Wilhelm C, Mustárdy L, Garab G (2008) Structurally flexible macro-organization of the pigment-protein complexes of the diatom *Phaeodactylum tricornutum*. Photosynth Res **95**: 237–245

Taddei L, Stella GR, Rogato A, Bailleul B, Fortunato AE, Annunziata R, Sanges R, Thaler M, Lepetit B, Lavaud J, (2016) Multisignal control of expression of the LHCX protein family in the marine diatom *Phaeodactylum tricornutum*. J Exp Bot **67**: 3939–3951

Tian L, Xu P, Chukhutsina VU, Holzwarth AR, Croce R (2017) Zeaxanthin-dependent nonphotochemical quenching does not occur in photosystem I in the higher plant *Arabidopsis thaliana*. Proc Natl Acad Sci USA **114**: 4828–4832

Ünlü C, Polukhina I, van Amerongen H (2016) Origin of pronounced differences in 77 K fluorescence of the green alga *Chlamydomonas reinhardtii* in state 1 and 2. Eur Biophys J **45**: 209–217

van der Weij-de Wit CD, Dekker JP, van Grondelle R, van Stokkum IHM (2011) Charge separation is virtually irreversible in photosystem II core complexes with oxidized primary quinone acceptor. J Phys Chem A **115**: 3947–3956

van Oort B, Murali S, Wientjes E, Koehorst RBM, Spruijt RB, van Hoek A, Croce R, van Amerongen H (2009) Ultrafast resonance energy transfer from a site-specifically attached fluorescent chromophore reveals the folding of the N-terminal domain of CP29. Chem Phys **357**: 113–119

van Stokkum IHM, Larsen DS, van Grondelle R (2004) Global and target analysis of time-resolved spectra. Biochim Biophys Acta **1657**: 82–104

van Stokkum IHM, Van Oort B, Van Mourik F, Gobets B, Van Amerongen H (2008) (Sub)-picosecond spectral evolution of fluorescence studied with a synchroscan streak-camera system and target analysis. *In* **TJ Aartsma, J Matysik**, eds, Biophysical Techniques in Photosynthesis. Springer, Dordrecht, The Netherlands, pp 223–240

Wientjes E, van Stokkum IHM, van Amerongen H, Croce R (2011) The role of the individual Lhcas in photosystem I excitation energy trapping. Biophys J **101**: 745–754

Wlodarczyk LM, Dinc E, Croce R, Dekker JP (2016) Excitation energy transfer in *Chlamydomonas reinhardtii* deficient in the PSI core or the PSII core under conditions mimicking state transitions. Biochim Biophys Acta **1857**: 625–633

Wu H, Cockshutt AM, McCarthy A, Campbell DA (2011) Distinctive photosystem II photoinactivation and protein dynamics in marine diatoms. Plant Physiol **156**: 2184–2195

Zhu SH, Green BR (2010) Photoprotection in the diatom *Thalassiosira pseudonana*: role of LI818-like proteins in response to high light stress. Biochim Biophys Acta **1797**: 1449–1457